Chinese Chemical Letters 35 (2024) 109847

Contents lists available at ScienceDirect

Chinese Chemical Letters

journal homepage: www.elsevier.com/locate/cclet

Metal-free diatomaceous carbon-based catalyst for ultrafast and anti-interference Fenton-like oxidation

Kexin Yin [a], Jingren Yang [c,*], Yanwei Li [b], Qian Li [a], Xing Xu [a,*]

[a] Shandong Key Laboratory of Water Pollution Control and Resource Reuse, School of Environmental Science and Engineering, Shandong University, Qingdao 266237, China
[b] Environment Research Institute, Shandong University, Qingdao 266237, China
[c] State Environmental Protection Key Laboratory of Environmental Health Impact Assessment of Emerging Contaminants, Shanghai Academy of Environmental Sciences, Shanghai 200233, China

ARTICLE INFO

Article history:
Received 13 December 2023
Revised 12 March 2024
Accepted 1 April 2024
Available online 3 April 2024

Keywords:
Peroxymonosulfate
Diatomite
Si-O doping
Fenton-like reaction
Electron transfer process (ETP)

ABSTRACT

Herein, a diatomite biomorphic Si-O doped carbon-based catalyst (DB-SiOC) was prepared using natural mineral diatomite as the silicon source and porous template. The results showed that the metal-free DB-SiOC catalyst exhibited ultrafast oxidation towards chlorophenol (CP) *via* peroxymonosulfate (PMS) activation, which was almost one order of magnitudes than most of carbon-based catalysts. The DB-SiOC/PMS system also showed the high ability to resist the interference of environmental matrix. The radicals ($^{\bullet}OH$ and $SO_4^{\bullet-}$) exhibited a very small contribution to the CP oxidation while the electron transfer processes (ETP) played the major role in the DB-SiOC/PMS system. The electron shuttles from the electron-donating CP molecules to the adjacent DB-SiOC/PMS* could be efficiently triggered *via* Si-O bonds as bridges, making it possible for ultrafast oxidation of CP. In addition, the hollow-disc shaped DB-SiOC provided the biomorphic DE structures with abundant pores for enriching the PMS and pollutants, thus further accelerating the oxidation reaction. This work provided a new routine for the fabrication of Si-O doped carbon-based catalysts with excellent Fenton-like catalytic activity, which would greatly promote their application prospects in Fenton-like systems.

In recent decades, the peroxymonosulfate-based advanced oxidation processes (PMS-AOPs) have attracted more and more attention in the degradation of refractory organic pollutants in water due to their ability to produce a variety of reactive oxygen species (ROS) and strong oxidation ability [1–3]. However, PMS itself exhibits limited efficacy in decomposing refractory organic pollutants, so it is imperative to explore suitable PMS activation strategies [4]. The addition of energy sources (such as ultraviolet irradiation and thermal treatment) or metal ions (including Fe^{2+}, Co^{2+}, Mn^{2+}, *etc.*) [5–7] has been found to activate PMS efficiently. Considering the high cost or potential secondary pollution associated with these methods, heterogeneous catalytic activation offers a promising alternative. Nevertheless, conventional heterogeneous catalysts used for activating PMS, such as transition metal oxides like CoO_x, FeO_x, $CuFe_2O_4$ [8–11], still encounter challenges related to metal leaching and limited catalytic stability when applied in practical scenarios.

Therefore, metal-free carbonaceous materials, such as graphene oxide, carbon nanotubes, and nanodiamonds have emerged as potential alternatives with the merits of abundant sources, non-toxicity and tunable physicochemical and electronic properties [12–14]. These carbon-based catalysts mainly rely on carbon configuration, oxygen functional groups, and heteroatomic doping as active sites [12,15,16], while their catalytic activity and stability still need to be further improved. Previous studies have demonstrated that doping heteroatoms with relatively weak electronegativity, such as N, B, O, or S, into the carbon skeleton could regulate the electronic structure, create new active sites, and dramatically boost the catalytic performance of carbonaceous materials consequently [17–19]. However, despite Si-O bonds exhibit weak electronegativity similar to N, B, and S elements [20], there are still few studies related to the activation of PMS *via* the carbon-based catalysts incorporated with the Si-O bonds so far.

Diatomite (DE), a common natural clay mineral mainly composed of amorphous silicon dioxide (SiO_2), exhibits unique features such as a three-dimensional porous and hollow structure, abundant silica hydroxyl groups, and low cost [21,22]. These properties make DE an attractive carrier or hard template for large-scale pro-

* Corresponding authors.
E-mail addresses: yangjr@saes.sh.cn (J. Yang), xuxing@sdu.edu.cn (X. Xu).

https://doi.org/10.1016/j.cclet.2024.109847
1001-8417/

duction of highly hierarchical and freestanding catalysts. For example, Dong *et al.* constructed two-dimensional $CoNi_3O_4$ nanoribbons with atomic layer-thickness on the abundant DE template [23]. The Cu nanoparticles were also anchored onto the DE to fabricate a freestanding three-dimensional catalyst [24]. Basically, the current literatures predominantly focus on utilizing DE as a carrier to support transition metal oxides or metal nanoparticles for efficient PMS activation [23,25], while neglecting the potential of exploiting DE as the template for fabricating carbon-based catalysts and subsequently achieving efficient PMS activation. The physicochemical properties of carbon-based catalysts derived from DE are highly dependant on the structural and compositional characteristics of DE [26,27]. On the one hand, carbon-based catalysts utilizing the three-dimensional hollow structure of DE could effectively address the issue of active site coverage resulting from layer-by-layer accumulation during synthesis. On the other hand, incorporating Si-O bonds into carbon-based catalysts can regulate its electronic structure and create new active sites, thereby significantly improving catalytic performance. Taking these aspects into account, it is of great significance to synthesize biomorphic carbonaceous materials assisted by DE templates for efficient activation of PMS.

In this work, a porous diatomite biomorphic Si-O doped carbon-based catalyst (DB-SiOC) was synthesized by dopamine-self polymerization using DE as sacrificial template (Fig. 1). The natural DE had a disc-shaped structure with the distribution of permeable pores between 200 nm and 400 nm (Fig. S1 in Supporting information). The dopamine monomers could polymerize on the surface of disc-shaped DE and form a disc-shaped poly-dopamine shell (DE@PDA). Thereafter, the Si-O bonds could be embedded in the carbon framework of DE@PDA *via* the pyrolysis at 800 °C to form the DE@DB-SiOC, and the DE core was removed by HF etching to obtain the DB-SiOC catalyst.

Scanning electron microscopy (SEM) and transmission electron microscopy (TEM) images unveiled that the DB-SiOC catalyst inherited the similar disc-shaped morphology (~20 μm) and porous structure (200–400 nm) as compared with that of DE (Figs. 2a and b). The energy dispersive spectrometer (EDS) showed that Si, O, N, and C atoms were uniformly distributed in the pore structure of DB-SiOC catalyst. In addition, the Si content in the DB-SiOC catalyst was 1.49 wt% detected by inductively coupled plasma optical emission spectroscopy (ICP-OES), which indicated that almost all the DE core have been successfully etched (Fig. S2 in Supporting information). In comparison, the nitrogen doped carbon (NC) derived from the same procedure except the addition of DE showed unique solid-sphere structures with a diameter of approximately 100 nm, which was quite different from that of the DB-SiOC (Fig. S3 in Supporting information). The BET specific surface area of DB-SiOC was up to 400.74 m^2/g (Table S1 in Supporting information), and it was almost 40–70 times higher than those of DE and DE@DB-SiOC although with the same pore structures; this indicated that the DB-SiOC was almost composed of residual hollow-disc carbon after HF etching of sacrificial DE. As exhibited in the Fourier Transform Infrared (FT-IR) spectra (Fig. 2c), the Si-O-Si asymmetric stretching vibration peaks of DE at 793 and 1113 cm^{-1} were hardly discernible in DB-SiOC [24,28], demonstrating the compositional difference between DE and DB-SiOC. Raman spectrum of DB-SiOC showed two distinct peaks at 1595 cm^{-1} (G-band) and 1352 cm^{-1} (D-band), which was similar to the NC and DE@DB-SiOC (Fig. S4 in Supporting information), further confirming the existence of a highly graphitized and defective carbon skeleton in DB-SiOC [29,30].

The compositions and chemical states of DB-SiOC can be further identified by the X-ray photoelectron spectroscopy (XPS). As shown in Fig. 3a, the Si composition in the DE was almost two orders of magnitude higher than that in DB-SiOC. The major peak (103.1 eV) in the XPS Si 2p of DE can be attributed to the Si-O bond (Fig. 3a), which corresponded well with the O 1s of DE (Fig. S5 in Supporting information) [31]. In contrast, this peak in DB-SiOC was significantly weakened as compared with that of DE, and a new peak at 102.1 eV can be observed in the Si 2p XPS spectrum of DB-SiOC, which was assigned to the Si-O-C bond [20,31]. The C composition in the DB-SiOC was extremely high (85.34 at%), as shown in Fig. 3b. In addition, the XPS C 1s can be deconvoluted into four fractions related to C–C, C–N, C=O, and O–C=O [32,33]. The DB-SiOC catalyst also showed a very small N composition (Fig. 3c), with graphitic N and pyridinic N as main N components doped in the carbon skeleton.

Catalytic performance of DB-SiOC/PMS system by compared with other catalytic systems was shown in Fig. 4a. The degradation efficiencies of *p*-chlorophenol (CP) were ~25% within 20 min in the PMS alone, NC/PMS, DE/PMS, and DE@DB-SiOC/PMS systems (Fig. 4a). In contrast, CP can be completely oxidized within 5 min in the DB-SiOC/PMS system with degradation rate (k_{obs}) of 0.945 min^{-1}, indicating that the DB-SiOC with Si-O doping could effectively promote PMS activation for pollutants oxidation. Spherical SiO_2 instead of DE was used as the template for the fab-

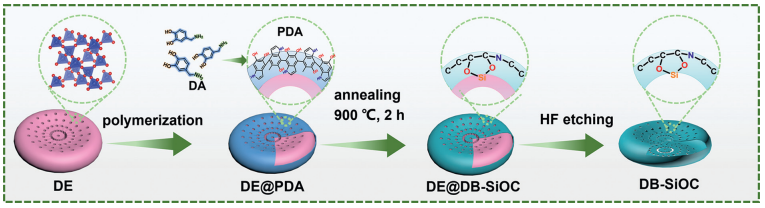

Fig. 1. Fabricating scheme of DB-SiOC.

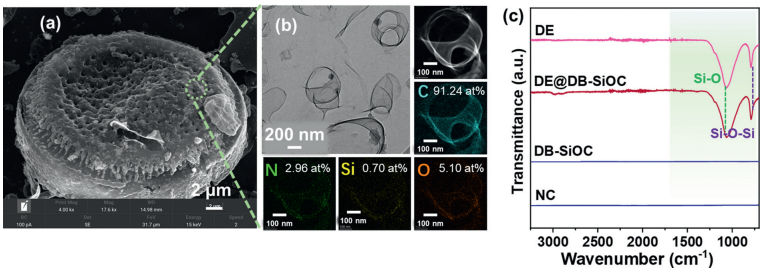

Fig. 2. (a) SEM image of DB-SiOC. (b) TEM images and EDS images of corresponding pore structure. (c) FT-IR spectra of different catalysts.

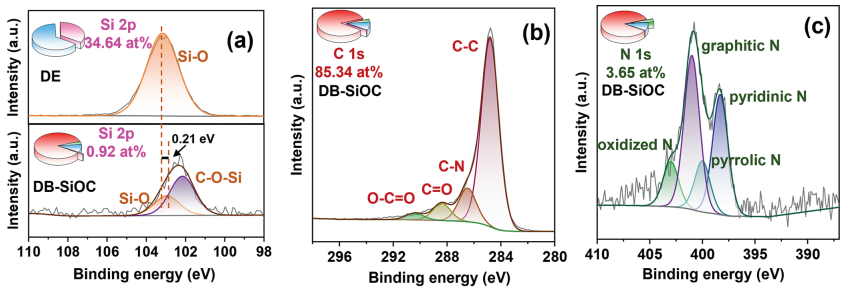

Fig. 3. (a) XPS Si 2p of DE and DB-SiOC. (b) XPS C 1s, and (c) N 1s of DB-SiOC.

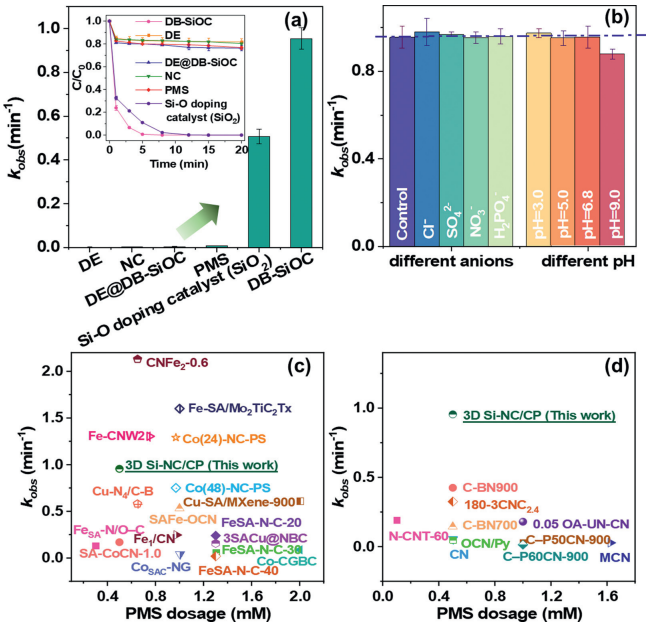

Fig. 4. (a) The k_{obs} values of CP oxidation by different catalysts. (b) Effects of different anions and pH on the degradation of CP. Comparison of k_{obs} values of as-prepared DB-SiOC with (c) single-atom catalysts, mM: mmol/L and (d) carbon-based catalysts reported in the literatures.

rication of universal Si-O doping catalyst. The Si-O doping catalyst derived from spherical SiO_2 exhibited the specific carbon-based XRD pattern, which was similar to that of DB-SiOC catalyst (Fig. S6 in Supporting information). The 100% degradation of CP by the Si-O doping catalyst (SiO_2) can also be achieved within 10 min with k_{obs} of 0.508 min^{-1} (Fig. S7 in Supporting information). This result showed the universality of excellent oxidation capacity of Si-O doping catalysts. The superior oxidation performance of DB-SiOC than that of Si-O doping catalyst (SiO_2) might be due to the biomorphic DE structure with abundant pores (200–400 nm) in DB-SiOC, which would promote the interaction of pollutants with active sites and accelerate the oxidation process [34].

The catalytic activity of DB-SiOC in versatile environmental matrixes (*e.g.*, Cl^-, SO_4^{2-}, NO_3^-, $H_2PO_4^-$) and a broad of pH conditions (3.0–9.0) was performed in Fig. 4b, Figs. S8 and S9 (Supporting information). The oxidation of CP by the DB-SiOC/PMS system almost kept constant with the co-existences of various anions, which indicated that its high ability to resist the interference of environmental matrixes. In addition, the degradation of CP was only marginally restrained as the pH was raised to 9.0; this might be due to that the surface of DB-SiOC was negatively charged at alkaline condition, which resulted in inhibitory effect on the adsorption of PMS and subsequent oxidation of CP due to the electrostatic repulsion. This can be confirmed by the point of zero charge (pH_{pzc}) of the DB-SiOC (Fig. S9b in Supporting information). In addition, the oxidation of CP could be comparable to the single-atom catalysts (Fig. 4c and Table S2 in Supporting information), and far exceeded the catalytic performances of most reported carbon-based catalysts (Fig. 4d and Table S3 in Supporting information).

The oxidation of CP in terms of DB-SiOC and PMS dosages (Figs. 5a and b) indicated that there was a positive correlation between the k_{obs} values and PMS dosages (>0.1 mmol/L) or DB-SiOC dosages (>0.04 g/L). In fact, more than 75% of CP could be oxidized by adding only 0.1 mmol/L of PMS (Fig. 5c), and the k_{obs} of CP oxidation by DB-SiOC could reach up to even 1.5–2.4 min^{-1} at PMS dosage of 1.0 mmol/L or DB-SiOC dosage of 0.14 g/L. This further confirmed the distinguished catalytic activity of DB-SiOC.

The generated ROS as well as the catalytic mechanisms of DB-SiOC with Si-O doping were investigated *via* a series of quenching experiments and electron paramagnetic resonance (EPR) instrument. The addition of EtOH and TBA showed little effect on the oxidation of CP (Fig. 6a and Fig. S10 in Supporting information). The EPR spectra using 5,5-dimethyl-1-pyrroline *N*-oxide (DMPO) as trapping agent exhibited the existence ofradical signals in the DB-SiOC/PMS system (Fig. 6b). This result indicated that some radicals ($^{\bullet}OH$ and $SO_4^{\bullet-}$) were generated and participated in the CP degradation, but was overwhelmed by specific nonradical pathway [35], which need to be further identified. It was reported that singlet oxygen ($^1O_2$) generated *via* PMS activation was an essential ROS for pollutant oxidation [36–39]. The $^1O_2$ signals were hardly discernible in the DB-SiOC/PMS system by using 2,2,6,6-teramethyl-4-piperidinol (TEMP) as trapping agent (Fig. 6b), which further verified that the contribution of $^1O_2$ on CP degradation was negligible.

To shed light on the electron-transfer process (ETP) regime in the DB-SiOC/PMS system, the galvanic oxidation system (GOS) was established by placing CP and PMS in two separate cells and connecting them with a salt bridge for evaluating electron transfer with the exclusion of other mechanisms (Fig. S11 in Supporting information). The DB-SiOC catalyst was coated on two graphite plate electrodes (20 mm × 20 mm × 3 mm) [40], and the current and degradation of CP were monitored in the GOS system (Fig. 6c). An extremely high instantaneous current (167.9 μA) was detected when PMS was added to the DB-SiOC based GOS system, which was ~3 times higher than those (55.5–66.9 μA) of other catalysts coated electrodes. Meanwhile, the degradation of CP *via* electron transfer in DB-SiOC based GOS system was also significantly higher than other GOS systems, suggesting that stronger ETP oxidation can be induced by the DB-SiOC/PMS system for the degradation of CP (Fig. S12 in Supporting information). This was also confirmed by the *i-t* curves in these catalytic systems, which showed the stronger current changes as the PMS and CP were added in the DB-SiOC/PMS system (Fig. S13 in Supporting information). The alternative of the adding orders of CP and PMS also showed significantly different current changes (Fig. 6d). The current of DB-SiOC decreased dramatically with the addition of PMS, which may be due to the role of electron redistribution derived from the gener-

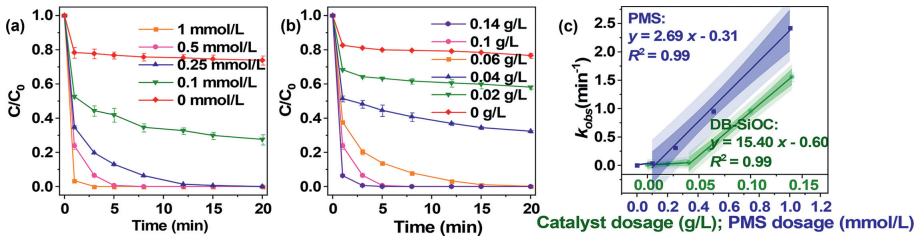

Fig. 5. (a) Catalytic activity of DB-SiOC at different (a) PMS dosages and (b) catalyst dosages (CP: 10 mg/L; PMS: 0.5 mmol/L; catalytic dosage: 0.1 g/L; pH 6.8). (c) Correlation between k_{obs} values and catalyst/PMS dosages.

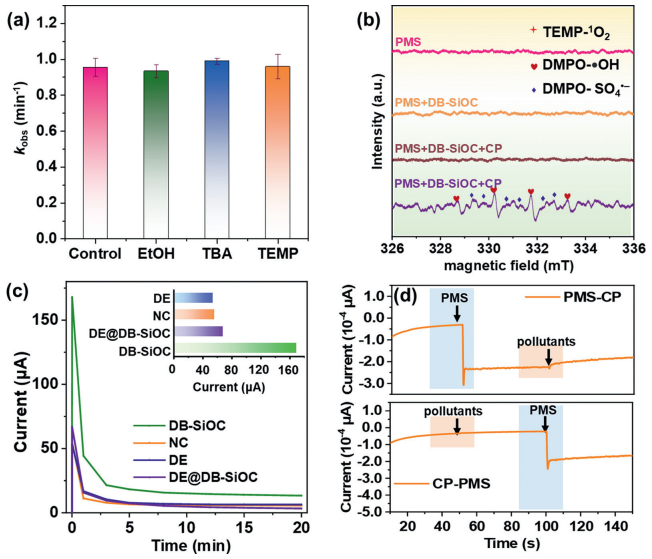

Fig. 6. (a) Different radical scavengers on the degradation of CP. (b) EPR spectra of the ROS generated in DB-SiOC/PMS system. (c) Current in GOS coating with different catalysts. (d) The *i-t* curves *via* changing the adding orders of PMS and pollutants using DB-SiOC as the working electrode.

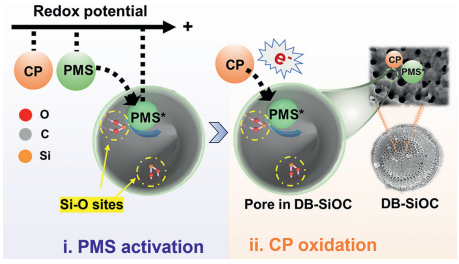

Fig. 7. Scheme of ETP oxidation towards the degradation of CP in the DB-SiOC/PMS system.

ated DB-SiOC/PMS* complex [41]. Conversely, no electron transfer occurred between the pollutant and DB-SiOC catalyst when CP was first injected into the DB-SiOC/PMS system.

In summary, this study provides a new strategy for the fabrication of high-efficiency carbon-based catalysts for PMS activation. The metal-free DB-SiOC catalyst exhibited exceptional Fenton-like catalytic activity and catalytic stability, and its catalytic oxidation activity was nearly one order of magnitude higher than those of various conventional carbon-based catalysts, even comparable to those of most single-atom catalysts. The radicals (•OH and $SO_4^{\bullet-}$) exhibited a very small contribution to the CP oxidation while the ETP pathway played the major role in the DB-SiOC/PMS system. The efficient electron transfer from the electron-donating CP molecules to the adjacent DB-SiOC/PMS* could be efficiently triggered, making it possible for ultrafast oxidation of CP (Fig. 7). In addition, the hollow-disc shaped DB-SiOC provided the biomorphic DE structures with abundant pores for enriching the PMS and pollutants, thus further accelerating the oxidation reaction.

Declaration of competing interest

The authors declare that they have no known competing financial interests or personal relationships that could have appeared to influence the work reported in this paper.

CRediT authorship contribution statement

Kexin Yin: Formal analysis, Resources, Validation, Visualization. **Jingren Yang:** Conceptualization, Supervision, Validation. **Yanwei Li:** Supervision, Validation. **Qian Li:** Conceptualization, Project administration, Software, Writing – review & editing. **Xing Xu:** Formal analysis, Investigation, Supervision, Writing – review & editing.

Acknowledgments

The work was supported by National Natural Science Foundation of China (No. 52170086), Shandong Provincial Excellent Youth (No. ZR2022YQ47). The authors also want to thank Conghua Qi from Shiyanjia Lab (www.shiyanjia.com).

Supplementary materials

Supplementary material associated with this article can be found, in the online version, at doi:10.1016/j.cclet.2024.109847.

References

[1] J. Lee, U. von Gunten, J.H. Kim, Environ. Sci. Technol. 54 (2020) 3064–3081.
[2] X. Wu, J.H. Kim, ACS ES&T Eng. 2 (2022) 1776–1796.
[3] Y. Jiang, D. Baimanov, S. Jin, et al., Proc. Natl. Acad. Sci. U. S. A. 120 (2023) e2210211120.
[4] J. Zhang, B. Jing, Z. Tang, et al., Appl. Catal. B: Environ. 289 (2021) 120023.
[5] Y. Su, M. Lu, R. Su, et al., Chin. Chem. Lett. 33 (2022) 2573–2578.
[6] Q. Zhao, C.C. Wang, P. Wang, Chin. Chem. Lett. 33 (2022) 4828–4833.
[7] J. Chen, C. Fang, W. Xia, et al., Environ. Sci. Technol. 52 (2018) 1461–1470.
[8] L. Peng, X. Duan, Y. Shang, et al., Appl. Catal. B: Environ. 287 (2021) 119963.
[9] Y.N. Shang, X. Xu, B.Y. Gao, et al., Chem. Soc. Rev. 50 (2021) 5281–5322.
[10] P.J. Duan, X. Xu, K.Y. Guo, et al., Appl. Catal. B: Environ. 316 (2022) 121695.
[11] Z.Y. Guo, R. Sun, Z. Huang, et al., Proc. Natl. Acad. Sci. U. S. A. 120 (2023) e2220608120.
[12] X. Wang, J. Jing, M. Zhou, R. Dewil, Chin. Chem. Lett. 34 (2023) 107621.
[13] L. Chen, C. He, R. Wang, et al., Chin. Chem. Lett. 32 (2021) 53–56.
[14] Y. Peng, G. Xie, P. Shao, et al., Appl. Catal. B: Environ. 310 (2022) 121345.
[15] W. Ren, L. Xiong, G. Nie, et al., Environ. Sci. Technol. 54 (2020) 1267–1275.
[16] X. Duan, H. Sun, Y. Wang, et al., ACS Catal. 5 (2014) 553–559.
[17] Y. Wang, Z. Zhang, Z. Yin, et al., Appl. Catal. B: Environ. 319 (2022) 121891.
[18] X. Duan, K. O'Donnell, H. Sun, et al., Small 11 (2015) 3036–3044.
[19] W. Ren, P. Zhou, G. Nie, et al., Water Res. 186 (2020) 116361.
[20] X. Dong, Z. Chen, A. Tang, et al., Adv. Funct. Mater. 32 (2022) 2111565.
[21] K. Li, X. Liu, T. Zheng, et al., Chem. Eng. J. 370 (2019) 136–147.
[22] K. Chen, C. Li, L. Shi, et al., Nat. Commun. 7 (2016) 13440.
[23] X. Dong, B. Ren, X. Zhang, et al., Appl. Catal. B: Environ. 272 (2020) 118971.
[24] J. Li, J. Xu, Z. Xie, et al., Adv. Mater. 30 (2018) e1800548.
[25] P. Xu, R. Wei, P. Wang, Water Res. 235 (2023) 119843.

[26] Y. Ding, Q. Cheng, J. Wu, et al., Adv. Mater. 34 (2022) e2202256.
[27] X. Wen, W. Feng, X. Li, et al., Adv. Mater. 35 (2023) e2211690.
[28] Z. Jia, T. Li, Z. Zheng, et al., Chem. Eng. J. 380 (2020) 122422.
[29] M. Zhang, H. Li, J. Chen, et al., Small 18 (2022) e2202476.
[30] X. Guo, Q. Zhang, H. He, et al., Appl. Catal. B: Environ. 335 (2023) 122886.
[31] J. Murata, K. Hayama, M. Takizawa, Appl. Surf. Sci. 625 (2023) 157190.
[32] Y. Chen, Z. Li, Y. Zhu, et al., Adv. Mater. 31 (2019) e1806312.
[33] G. Chen, P. Liu, Z. Liao, et al., Adv. Mater. 32 (2020) e1907399.
[34] A. Wang, J. Ni, W. Wang, et al., Appl. Catal. B: Environ. 319 (2022) 121926.
[35] X. Duan, H. Sun, Z. Shao, et al., Appl. Catal. B: Environ. 224 (2018) 973–982.
[36] T. Liu, S. Xiao, N. Li, et al., Nat. Commun. 14 (2023) 2881.
[37] Y. Yang, G. Banerjee, G.W. Brudvig, et al., Environ. Sci. Technol. 52 (2018) 5911–5919.
[38] B. Liu, W. Guo, W. Jia, et al., Water Res. 201 (2021) 117313.
[39] A. Wang, B.Z. Zhu, C.H. Huang, et al., Water Res. 235 (2023) 119904.
[40] J. Peng, P. Zhou, H. Zhou, et al., Environ. Sci. Technol. 55 (2021) 9189–9198.
[41] X. Zhou, M.K. Ke, G.X. Huang, et al., Proc. Natl. Acad. Sci. U. S. A. 119 (2022) e2119492119.